

Article

Analysis of the Notch Filter Insertion Position for Natural Frequency Vibration Suppression in a Magnetic Suspended Flywheel Energy Storage System

Hongjin Hu ^{1,†}, Jingbo Wei ^{1,†} , Haoze Wang ², Peng Xiao ¹, Yuan Zeng ¹  and Kun Liu ^{1,*}¹ School of Aeronautics and Astronautics, Sun Yat-Sen University, Shenzhen 518107, China² School of Civil Aviation, Northwestern Polytechnical University, Suzhou 215400, China

* Correspondence: liukun6@mail.sysu.edu.cn

† These authors contributed equally to this work.

Abstract: The composite material flywheel rotor of a flywheel energy storage system (FESS) has a low natural frequency. When the system suffers from noise interference, the magnetic bearing generates a force with the same frequency as the natural frequency and causes vibration to occur. Thus, it is necessary to suppress the natural vibration of the magnetic suspended (MS) FESS. The LMS adaptive notch filter is generally adopted for vibration suppression. The vibration suppression performance of the system is different when the insertion position of the notch filter is different. This paper analyzes the influence of the notch filter in different insertion positions of the control system. Through the transfer function from noise to magnetic bearing force, theoretical analysis of the influence of different positions of the notch filter is performed. Corresponding experiments are performed in a 500 kW MS FESS prototype. The theoretical analysis is verified experimentally.

Keywords: magnetic suspension flywheel energy storage; natural frequency; vibration suppression; insertion position of the notch filter



Citation: Hu, H.; Wei, J.; Wang, H.; Xiao, P.; Zeng, Y.; Liu, K. Analysis of the Notch Filter Insertion Position for Natural Frequency Vibration Suppression in a Magnetic Suspended Flywheel Energy Storage System. *Actuators* **2023**, *12*, 22. <https://doi.org/10.3390/act12010022>

Academic Editor: Kirill Poletkin

Received: 8 December 2022

Revised: 28 December 2022

Accepted: 30 December 2022

Published: 4 January 2023



Copyright: © 2023 by the authors. Licensee MDPI, Basel, Switzerland. This article is an open access article distributed under the terms and conditions of the Creative Commons Attribution (CC BY) license (<https://creativecommons.org/licenses/by/4.0/>).

1. Introduction

Energy storage systems (ESSs) play increasingly important roles in modern industrial applications. A flywheel energy storage system (FESS) is a type of ESS that has the advantages of high efficiency, fast response, instantaneous high power, low maintenance, and long life [1–3]. Thus, FESSs have been applied in electric vehicles [4,5], hydraulic excavators [6], wind power generation [7,8], microgrids [9], photovoltaic generation [10], uninterruptible power supply (UPS) [11,12], and aerospace applications [13]. In an FESS, energy is stored in a high-speed flywheel rotor. The FESS generally adopts a composite material flywheel rotor [14,15]. By using a composite flywheel rotor, the FESS can obtain a higher linear velocity and energy storage density [15]. However, the stiffness of the composite material is small, resulting in a relatively low natural frequency of the composite flywheel, which is generally a few hundred hertz. In the magnetic suspended (MS) FESS, the composite material flywheel rotor is supported by magnetic bearings (MBs), which have the advantages of low loss, frictionlessness, and silent operation [16,17]. The MB controller generates noise interference of the same frequency as the natural frequency of the flywheel rotor. Therefore, the MB generates an electromagnetic force that has the same frequency as the natural frequency. This electromagnetic force becomes the excitation source of the flywheel rotor. When the frequency of the force is the same as the natural frequency, the flywheel rotor vibrates violently, causing system instability [18].

The notch filter can filter out signals with a certain frequency. Therefore, the vibration of the MB system can be suppressed. Vibration suppression methods based on notch filters have been widely applied in MB systems. The main notch filters applied in MB systems include the generalized notch filter [19,20], the least mean square (LMS) adaptive notch filter [21–23], and the phase-shift notch filter [24,25]. In [19], a generalized narrow-band notch filter is proposed for an MB system. This notch filter is inserted into the multivariable feedback without destabilizing the closed loop. In [20], a generalized notch filter based on synchronous rotating frame (SRF) transformation is proposed for autobalancing of the magnetically suspended rotor. In [21], a harmonic based on a frequency-domain adaptive LMS is proposed to suppress the vibration force. This method introduces a convergence factor in the frequency domain that improves the updating strategy of the step size and the convergence rate of the algorithm. In [22], a double-channel adaptive LMS error algorithm is proposed to suppress the imbalanced vibration. A modified adaptive notch filter with phase shift is proposed in [23] to suppress the unbalanced vibration. This notch filter does not require angular velocity information. In [24], a phase-shift notch filter is proposed to ensure stable operations over the entire speed range. In [25], a control system scheme with cascaded mode phase-shift notch filters is proposed for the MB rotor control system.

Notch filters have been widely applied in the vibration suppression of MB systems and show satisfactory vibration suppression performance. However, research on the notch filters in MB control systems is mainly focused on the notch filter algorithm. The influence of the insertion positions of the notch filters is not sufficiently discussed. The MB control system is a double closed-loop system. The outer loop is a position control loop, and the inner loop is a current control loop. The notch filter can be inserted into the feedback path of the outer loop, the forward path of the outer loop, the feedback path of the inner loop, and the forward path of the inner loop. In general, the notch filter is inserted into the forward path of the position control loop. In this paper, the influence of the notch filter access position is analyzed, and the control model of the MB system is clarified. The LMS adaptive notch filter is adopted for vibration suppression, and the influence of the insertion position of the notch filter is analyzed through the Bode plot.

The remainder of this paper is organized as follows. In Section 2, the structure of the MS FESS is presented. In Section 3, the influence of the access position of the notch filter is analyzed. In Section 4, the experiment is performed on the FESS prototype to verify the theoretical analysis. Finally, the conclusion is drawn in Section 5.

2. Structure of the FESS

An FESS is a type of mechanical energy storage device in which mechanical energy is stored in a high-rotation-speed flywheel rotor. The structure of the MS FESS is shown in Figure 1. The MS FESS is installed vertically, which mainly includes the flywheel rotor, MBs, high-speed motor, corresponding position sensors, and base. The flywheel rotor is supported by MBs and installed in a vacuum chamber. Thus, the flywheel rotor can operate at a high speed without mechanical friction and with low wind resistance. FESS achieves energy conversion through a high-speed motor. The motor rotor connects to the flywheel rotor. The flywheel rotor has the same rotation speed as the rotor of the motor. The FESS has three MBs as follows: the top radial MB, the bottom radial MB, and the top axial MB. The power amplifier (PA) should generate currents to the MBs of the FESS. By applying the appropriate current, the MB system can generate the corresponding electromagnetic force to suspend the flywheel rotor.

Stable MS control is important to the MS FESS. Natural frequency vibration is one of the issues that cause system instability. To avoid natural frequency vibration, the force with the same frequency as the natural frequency should be filtered out.

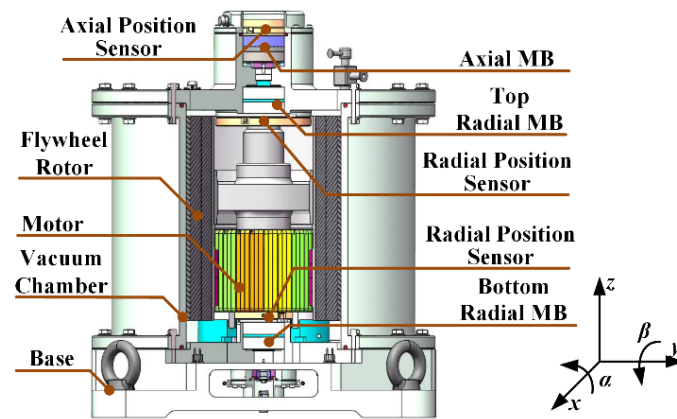


Figure 1. The structure of the FESS.

3. Analysis of the Insertion Position of the Notch Filter

In this section, the influence of the insertion position of the notch filter is analyzed. The model of the MB control system and the LMS adaptive notch filter are presented. Based on the control model and the notch filter, the influence of the insertion position of the notch filter is analyzed through a Bode plot.

3.1. Model of the Magnetic Bearing Control System

The MS FESS of Figure 1 adopts a permanent-magnet-biased MB. The structure diagram of the hybrid MB is shown in Figure 2. The electromagnetic force generated by the hybrid MB is deduced as Equation (1):

$$f_{mag} = \frac{\mu_0 S N^2}{2} \left[\left(\frac{I_0 - I}{D_0 - x} \right)^2 - \left(\frac{I_0 + I}{D_0 + x} \right)^2 \right] \quad (1)$$

where f_{mag} is the electromagnetic force of the MB, N is the number of turns of the MB coil, μ_0 is the vacuum permeability, S is the area directly opposite to the magnetic pole, D_0 is the MB air gap, x is the flywheel rotor position, and I is the coil current.

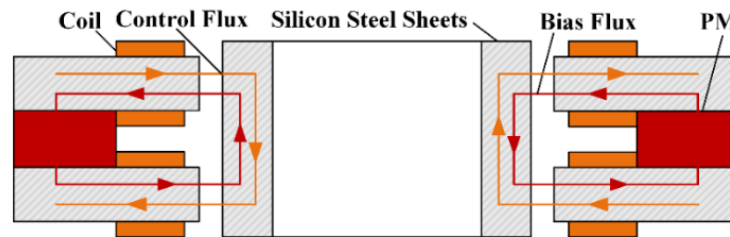


Figure 2. The structure diagram of the hybrid MB.

The rotor is suspended at the position where $x = 0$. According to the Taylor series expansion, Equation (1) can be linearized as follows in Equation (2):

$$f_{mag} = K_x x + K_i I \quad (2)$$

where K_x is the displacement stiffness of the MB and K_i is the current stiffness of the MB.

According to Newton's second law, the kinematic equation can be deduced as follows in Equation (3):

$$f_{mag} = m \ddot{x} = K_x x + K_i I \quad (3)$$

The transfer function of Equation (3) is presented as follows:

$$G_m(s) = \frac{K_i}{ms^2 - K_x}. \quad (4)$$

The MS control system is a double closed-loop control system. The control block diagram is shown in Figure 3. A proportional–derivative (PD) controller is adopted for MB position control, and the transfer function of the PD controller is presented as follows in Equation (5):

$$G_{pd}(s) = K_{px} + K_{dx}s \tag{5}$$

where K_{px} is the proportional coefficient of the PD controller and K_{dx} is the differential coefficient of the PD controller.

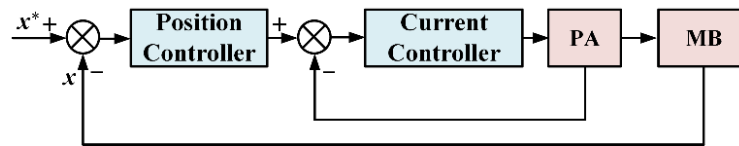


Figure 3. Control block diagram of the MS control.

For current control, the coil of the MB is equivalent to the resistance–inductance series circuit. Thus, the model of the coil can be deduced as follows in Equation (6):

$$G_c(s) = \frac{1}{Ls + R} \tag{6}$$

where L is the inductance of the MB coil and R is the resistance of the MB coil.

A (proportional integral) PI controller is generally used for current control, and the transfer function of the PI controller is deduced as follows in Equation (7):

$$G_{pi}(s) = K_{pi} + \frac{K_{ji}}{s} \tag{7}$$

The influence of the insertion position of the notch filter is analyzed based on the above control system model.

3.2. LMS Adaptive Notch Filter Algorithm

The vibration is suppressed by the LMS adaptive notch filter. The LMS adaptive notch filter is based on the Wiener filter and minimum mean square error (MMSE) criteria, which uses the gradient descent method to minimize the mean square error of the signal [26]. Thus, the filter can output the best signal estimate. The block diagram of the LMS adaptive filter is shown in Figure 4. In Figure 4, T_s is the sampling time of the discrete system, ω_0 is the center frequency of the LMS notch filter, the input vector $\mathbf{X}(kT_s)$ is the reference signal of the algorithm, $d(kT_s)$ is the expected signal, and w is the weighting coefficient of the filter.

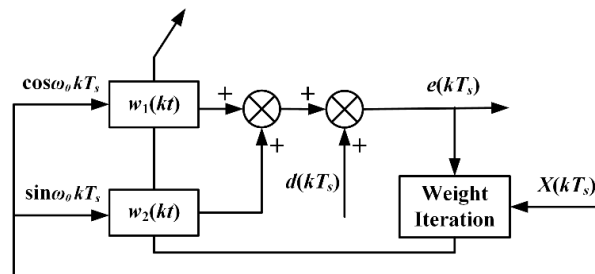


Figure 4. The block diagram of the LMS notch filter.

The weighting coefficient is adjusted by the gradient descent method to minimize the mean square error. The mean square error is presented as follows in Equation (8):

$$MSE = E \left[e^2(kT_s) \right] \tag{8}$$

The error of the signal can be deduced as follows in Equation (9):

$$e(kT_s) = d(kT_s) - \mathbf{X}^T(kT_s)\mathbf{W}(kT_s)\mathbf{X}(kT_s) \tag{9}$$

where \mathbf{W} is the filter weighting coefficient matrix.

Combining (8) and (9), the mean square error can be further deduced as follows in Equation (10).

$$MSE = E(d^2) + \mathbf{W}^T\mathbf{R}\mathbf{W} - 2\mathbf{W}^T\mathbf{P} \tag{10}$$

where \mathbf{R} is the autocorrelation matrix of the input signal, \mathbf{P} is the cross-correlation matrix of the expected signal $d(kT_s)$, and $\mathbf{X}(kT_s)$ is the input signal.

The partial differential of the mean square error can be deduced as follows in Equation (11).

$$\frac{\partial MSE}{\partial \mathbf{W}} = 2\mathbf{R}\mathbf{W} - 2\mathbf{P} \tag{11}$$

According to Equation (11), the filter coefficient matrix \mathbf{W} can be directly calculated. However, the inverse matrix of \mathbf{R} needs to be obtained. In practical applications, matrix inversion requires massive computing resources. Thus, the descent method is adopted to obtain the filter weighting matrix. The weighting matrix is adjusted along the negative gradient direction. The recursive equations of the LMS adaptive notch filter algorithm can be deduced as follows in Equation (12) [26]:

$$\begin{cases} e(kT_s) = d(kT_s) - y(kT_s) \\ y(kT_s) = w_1(kT_s) \cos \omega_0 kT_s + w_2(kT_s) \sin \omega_0 kT_s \\ W[(k+1)T_s] = W(kT_s) + 2\mu e(kT_s)X(kT_s) \end{cases} \tag{12}$$

where μ is the step length.

The step length can be used to adjust the convergence speed and steady-state accuracy of the filter. According to Equation (12), the transfer function of the LMS adaptive notch filter can be deduced as follows in Equation (13):

$$G_f(z) = \frac{1 - 2z^{-1} \cos \omega_0 T_s + z^{-2}}{1 - 2(1 - \mu)z^{-1} \cos \omega_0 T_s + (1 - 2\mu)z^{-2}} \tag{13}$$

In this paper, the LMS adaptive notch filter of Equation (13) is used to analyze the influence of the notch filter at different insertion positions of the control system on vibration suppression.

3.3. Insertion Position of the Notch Filter

The MS control system is a double closed-loop system. The LMS adaptive notch filter has four insertion positions. The four insertion positions are the forward path of the outer loop, the feedback path of the outer loop, the forward path of the inner loop, and the feedback path of the inner loop, which are shown in Figure 5.

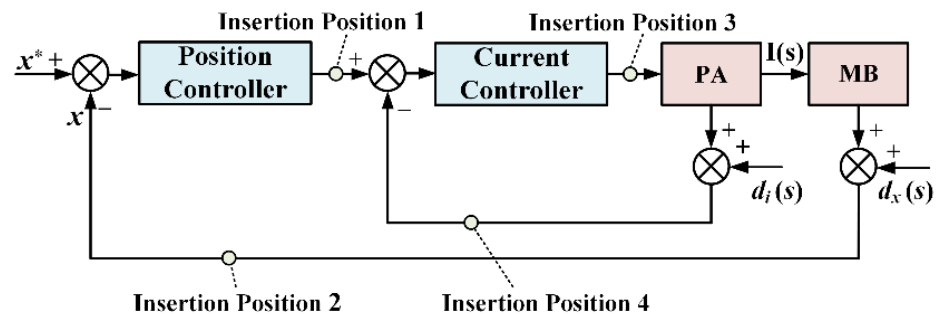


Figure 5. Control block diagram with four notch filter insertion positions.

According to Equation (2), the electromagnetic force of the MB is proportional to the current of the PA. When the PA generates a current that has the same frequency as the natural frequency of the flywheel rotor and has a sufficiently large amplitude, a violent vibration occurs in the flywheel rotor. To suppress the vibration, the PA should not generate a current that has the same frequency as the natural frequency. In MS control, signals with the same frequency as the natural frequency mainly come from the noise of the position sensors and the current sensor. To analyze the influence of different insertion points on vibration suppression, the transfer function from the sensor noise to the PA current is deduced. Based on the transfer function, this paper uses a Bode plot to qualitatively analyze the influence of different insertion positions.

When the notch filter is inserted at position 1, i.e., the forward path of the outer loop, the transfer function from the sensor noise to the current can be deduced as follows in Equations (14) and (15):

$$G_{1i}(s) = \frac{I(s)}{d_i(s)} = \frac{G_{pi}(s)G_c(s)}{1 + G_{pd}(s)G_{pi}(s)G_c(s)G_m(s)G_f(s) + G_{pi}(s)G_c(s)} \quad (14)$$

$$G_{1x}(s) = \frac{I(s)}{d_x(s)} = \frac{G_f(s)G_{pd}(s)G_{pi}(s)G_c(s)}{1 + G_{pd}(s)G_{pi}(s)G_c(s)G_m(s)G_f(s) + G_{pi}(s)G_c(s)} \quad (15)$$

where $G_f(s)$ is the continuous transfer function of the LMS adaptive notch filter, $d_i(s)$ is the Laplace transform of the current noise signal, $d_x(s)$ is the Laplace transform of position noise, and $I(s)$ is the Laplace transform of the current.

The Bode plots of Equations (14) and (15) are shown in Figure 6. According to Figure 6, the natural frequency noise of the position sensor can be filtered out when the notch filter is inserted at position 1. However, the natural frequency noise of the current sensor cannot be filtered out.

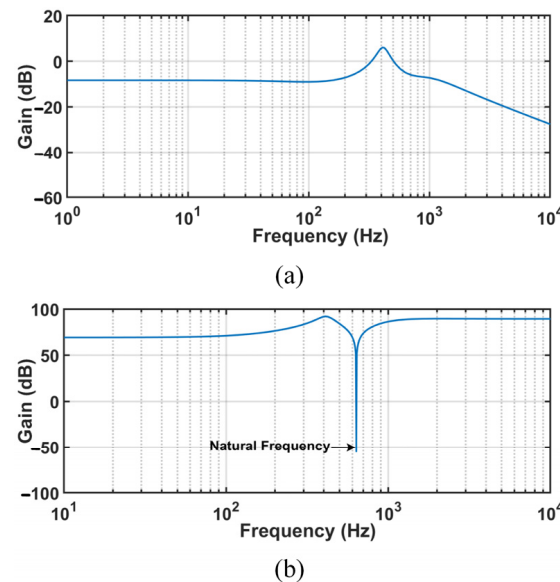


Figure 6. Bode plot of the transfer function from the noise to the currents of insertion positions 1 and 2: (a) transfer function from the current noise to the current; (b) transfer function from the position noise to the current.

When the notch filter is inserted into position 2, the transfer function from the sensor noise to the current is deduced as follows in Equations (16) and (17).

$$G_{2i}(s) = \frac{I(s)}{d_i(s)} = \frac{G_{pi}(s)G_c(s)}{1 + G_{pd}(s)G_{pi}(s)G_c(s)G_m(s)G_f(s) + G_{pi}(s)G_c(s)} \quad (16)$$

$$G_{2x}(s) = \frac{I(s)}{d_x(s)} = \frac{G_f(s)G_{pd}(s)G_{pi}(s)G_c(s)}{1 + G_{pd}(s)G_{pi}(s)G_c(s)G_m(s)G_f(s) + G_{pi}(s)G_c(s)} \quad (17)$$

According to Equations (14)–(17), the transfer functions of insertion position 1 and insertion position 2 are the same. Thus, the Bode plots of insertion position 1 and insertion position 2 are the same.

When the notch filter is inserted at position 3, the transfer function from the sensor noise to the current is deduced as follows in Equations (18) and (19).

$$G_{3i}(s) = \frac{I(s)}{d_i(s)} = \frac{G_f(s)G_{pi}(s)G_c(s)}{1 + G_{pd}(s)G_{pi}(s)G_c(s)G_m(s) + G_{pi}(s)G_c(s)G_f(s)} \quad (18)$$

$$G_{3x}(s) = \frac{I(s)}{d_x(s)} = \frac{G_f(s)G_{pd}(s)G_{pi}(s)G_c(s)}{1 + G_{pd}(s)G_{pi}(s)G_c(s)G_m(s) + G_{pi}(s)G_c(s)G_f(s)} \quad (19)$$

The Bode plots of Equations (18) and (19) are shown in Figure 7. When the notch filter is inserted at position 3, the natural frequency noise of the position sensor and the current sensor can both be filtered out.

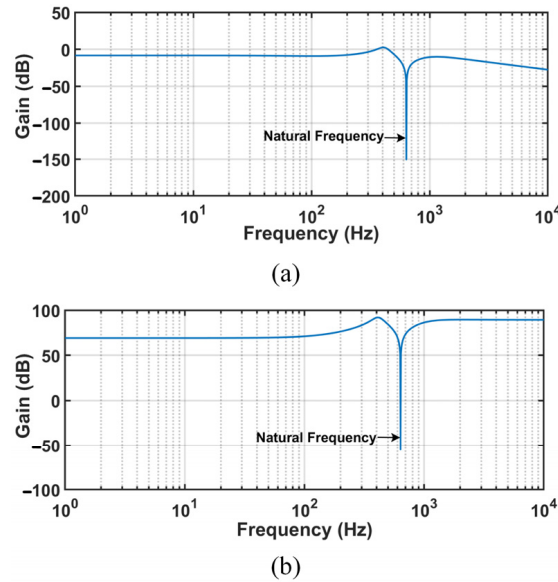


Figure 7. Bode plot of the transfer function from the noise to the current of insertion position 3: (a) transfer function from the current noise to the current; (b) transfer function from the position noise to the current.

When the notch filter inserts to position 4, the transfer function from the sensor noise to the current is deduced as follows in Equations (20) and (21):

$$G_{4i}(s) = \frac{I(s)}{d_i(s)} = \frac{G_f(s)G_{pi}(s)G_c(s)}{1 + G_{pd}(s)G_{pi}(s)G_c(s)G_m(s) + G_{pi}(s)G_c(s)G_f(s)} \quad (20)$$

$$G_{4x}(s) = \frac{I(s)}{d_x(s)} = \frac{G_{pd}(s)G_{pi}(s)G_c(s)}{1 + G_{pd}(s)G_{pi}(s)G_c(s)G_m(s)G_f(s) + G_{pi}(s)G_c(s)G_f(s)} \quad (21)$$

The Bode plots of Equations (20) and (21) are shown in Figure 8. According to Figure 8, the natural frequency noise of the current sensor can be filtered out when the notch filter is inserted at position 4. However, the natural frequency noise of the position sensor cannot be filtered out.

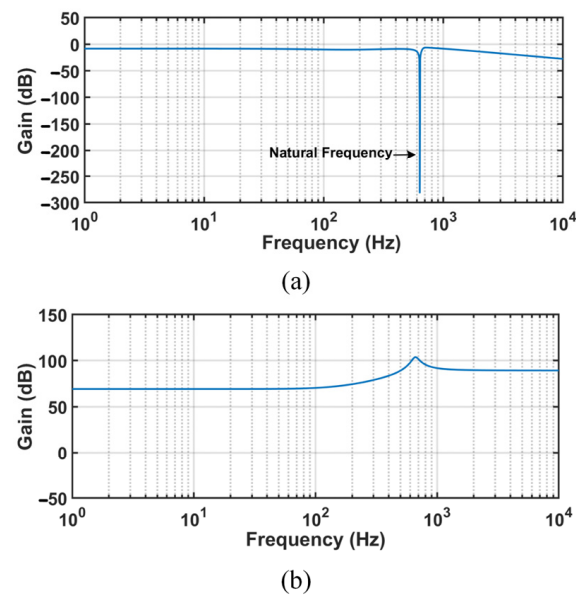


Figure 8. Bode plot of the transfer function from the noise to the current of insertion position 4: (a) transfer function from the current noise to the current; (b) transfer function from the position noise to the current.

Based on the above analysis, the notch filter is inserted at position 3, i.e., the forward path of the inner loop is the most effective to filter out the natural frequency noise of the sensors.

4. Experimental Results

The influence of the insertion position of the LMS adaptive notch filter is experimentally analyzed on a 500-kW MS FESS prototype. The natural frequency is tested through a laser vibrometer. The position responses of different insertion positions of the notch filter are tested.

4.1. Experimental Platform

The experimental platform is shown in Figure 9. The experimental platform includes a 500-kW MS FESS prototype, Tektronix oscilloscope, Rohde & Schwarz FSH4 dynamic signal analyzer, and power supply. The MS FESS prototype is shown in Figure 10, and its main parameters are listed in Table 1.



Figure 9. The experimental platform of the MS FESS.

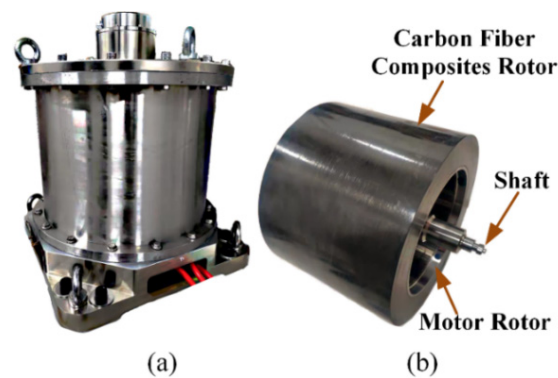


Figure 10. (a) The MS FESS prototype. (b) The flywheel rotor.

Table 1. Main Parameter Specification of the MS.

Symbol	Description	Value
V_{DC}	Maximum voltage	500 V
P_r	Maximum power	500 kW
E_m	Stored energy	1.2 kWh
ω_m	Maximum design speed	27,000 rpm
M_r	Rotor weight	58.0 kg
S_m	Prototype Size	$\Phi 500 \times 590$ mm

4.2. Experiment A: Test of the Natural Frequency of the Flywheel Rotor

The natural frequency test device is shown in Figure 11. The flywheel rotor is suspended by a rope. A Polytecpsv-500 laser vibrometer is used to test the natural frequency. The tested natural frequency is shown in Figure 12. According to Figure 12, the natural frequency of the flywheel rotor is 635 Hz. Thus, the selected center frequency of the notch filter is 635 Hz.

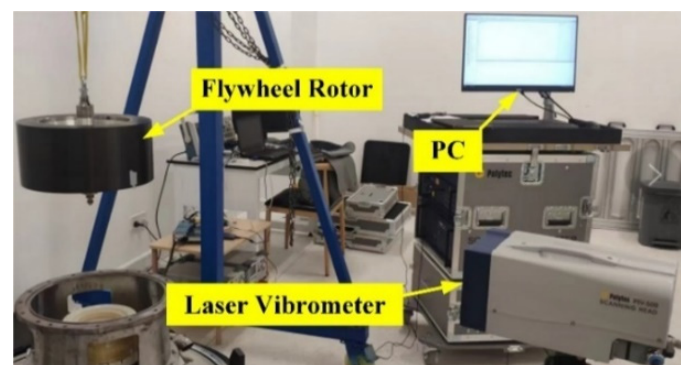


Figure 11. The device for testing the natural frequency of the flywheel rotor.

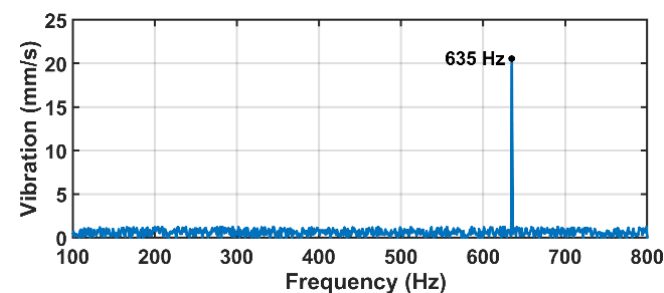


Figure 12. The tested natural frequency of the flywheel rotor.

The frequency analysis of the current sensor signal and position sensor signal is presented in Figure 13. The frequency analysis shows that the current sensor signal and position sensor signal include a noise signal that is the same as the natural frequency. To avoid natural frequency vibration, the noise signal that is the same as the natural frequency should be filtered out.

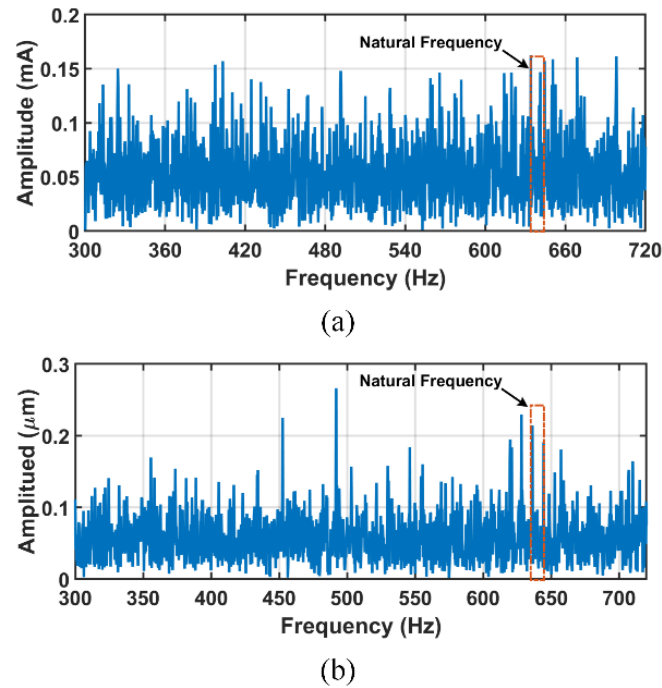


Figure 13. Frequency analysis of the sensor signal: (a) current sensor; (b) position sensor.

4.3. Experiment B: Position Responses of Different Insertion Positions

The experimental analysis of different insertion positions of the notch filter is performed. The parameters of the notch filter are listed in Table 2. Figure 14 shows the experimental results when the notch filter is inserted into the forward path of the outer loop, i.e., insertion position 1. According to Figure 14a, the amplitude of the vibration without a notch filter is larger than 25 μm. With a notch filter, the amplitude of the vibration can be smaller than 4 μm. The experimental result illustrates that the vibration can be suppressed when the notch filter is inserted at position 1. However, the notch filter cannot filter out the natural frequency noise of the current sensor. When the gain of the current controller increases, the current noise is amplified. Figure 14b shows the position response curve when the gain of the current controller is increased by 30%. The amplitude of the vibration is increased and is larger than 10 μm.

Table 2. Main Parameters of the LMS filter.

Symbol	Description	Value
ω_0	Center frequency	635 Hz
μ	Step length	0.01
f_s	Sampling frequency	5 kHz

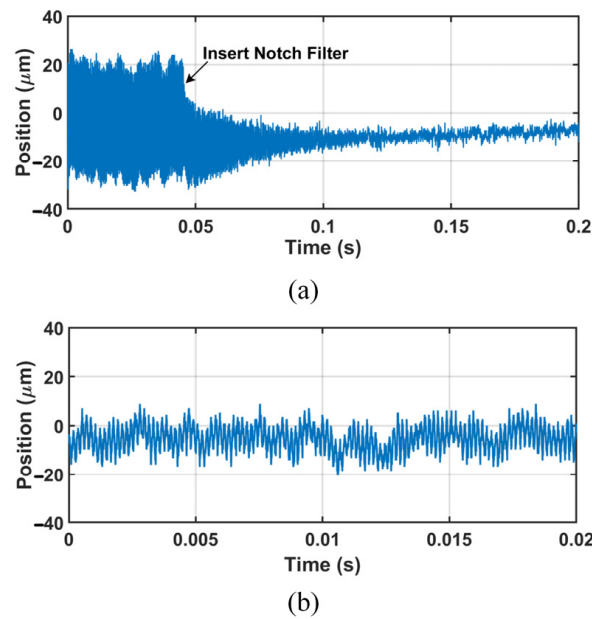


Figure 14. The experimental results when the notch filter is inserted at position 1: (a) position signal when the notch filter is inserted; (b) position signal when the gain of the current controller increases.

Figure 15 shows the experimental results when the notch filter is inserted into the feedback path of the outer loop, i.e., insertion position 2. With this notch filter, the vibration can be suppressed, and the amplitude of the vibration is smaller than $4\ \mu\text{m}$. Similar to insertion at position 1, the notch filter cannot filter out the natural frequency noise of the current sensor. Figure 15b shows the position response curve when the gain of the current controller is increased by 30%. The amplitude of the vibration is increased and is larger than $12\ \mu\text{m}$.

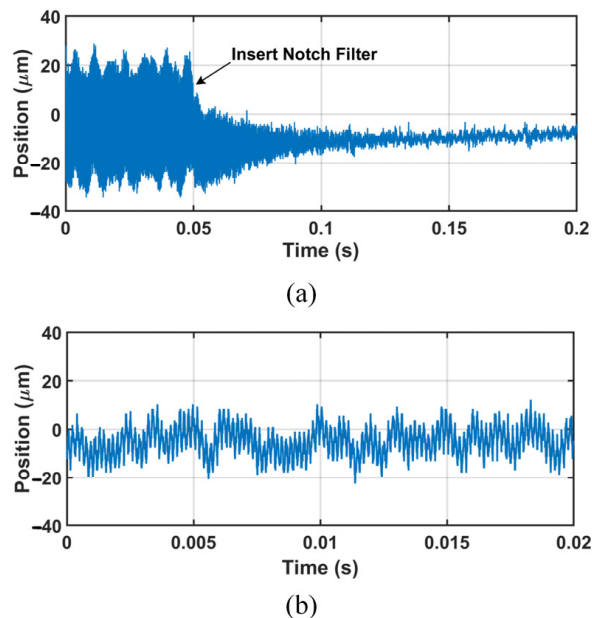


Figure 15. The experimental results when the notch filter is inserted at position 2: (a) position signal when the notch filter is inserted; (b) position signal when the gain of the current controller increases.

Figure 16 shows the experimental results when the notch filter is inserted into the forward path of the inner loop, i.e., insertion position 3. With a notch filter, the amplitude of the vibration can be suppressed and is smaller than $4\ \mu\text{m}$. Based on the theoretical

analysis, the notch filter can filter out the natural frequency noise of the current sensor and the position sensor. Figure 16b shows the position response curve when the gain of the position controller is increased by 30%. The amplitude of the vibration does not significantly increase and is smaller than $6\ \mu\text{m}$.

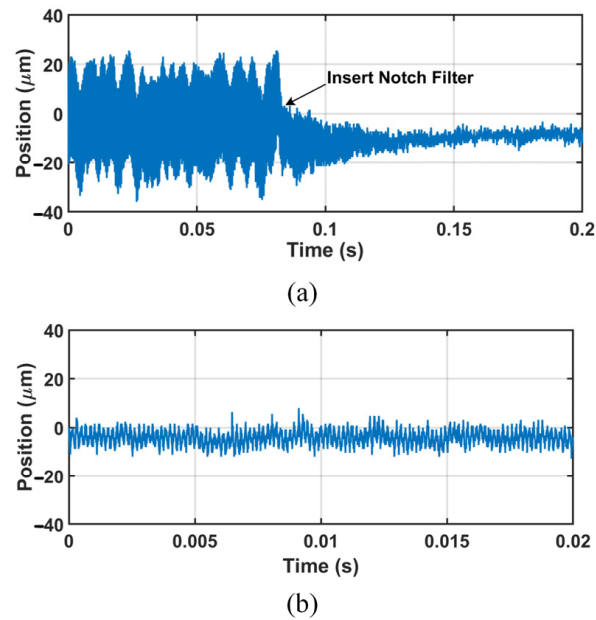


Figure 16. The experimental results when the notch filter is inserted at position 3: (a) position signal when the notch filter is inserted; (b) position signal when the gain of the position controller increases.

Figure 17 shows the experimental results when the notch filter is inserted into the feedback path of the inner loop, i.e., insertion position 4. With a notch filter, the vibration can be suppressed, and the amplitude of the vibration is smaller than $4\ \mu\text{m}$. The notch filter cannot filter out the natural frequency noise of the position sensor. Figure 17b shows the position response curve when the gain of the position controller is increased by 30%. The amplitude of the vibration is increased and is larger than $18\ \mu\text{m}$.

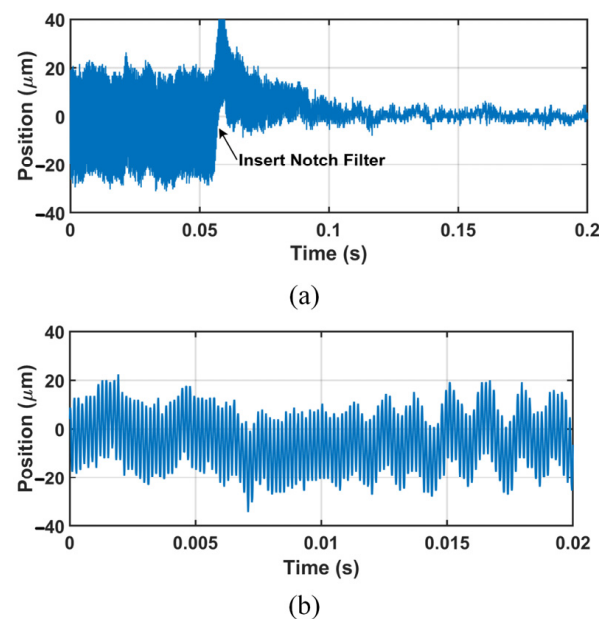


Figure 17. The experimental results when the notch filter is inserted at position 2: (a) position signal when the notch filter is inserted; (b) position signal when the gain of the position controller increases.

The experimental results show that the vibration can be suppressed to a certain extent by inserting the notch filter into the four positions of Figure 5. When the notch filter is inserted at position 3, the MS system shows the most appropriate vibration suppression performance. The experimental results match the theoretical analysis.

5. Conclusions

In this paper, the influence of the insertion position of the notch filter in an MS FESS is analyzed for natural frequency vibration suppression. The MS control model and LMS adaptive notch filter are given. Based on the control mode and notch filter, the influence of the insertion position is analyzed by the Bode plot. The experimental analysis is carried out on a 500 kW MS FESS prototype. The main conclusions are presented as follows.

- (1) The vibration can be suppressed to some extent by inserting the notch filter into the forward and feedback path of the outer loop and the forward and feedback path of the inner loop.
- (2) When the notch filter is inserted into the forward and feedback path of the outer loop, the natural frequency noise of the position sensor can be filtered out; nevertheless, the natural frequency noise of the current sensor cannot be filtered out. When the notch filter is inserted into the feedback path of the inner loop, the natural frequency noise of the position sensor can be filtered out; nevertheless, the natural frequency noise of the current sensor cannot be filtered out.
- (3) When the notch filter is inserted into the forward path of the inner loop, the natural frequency noise of the position sensor and current sensor can be filtered out. Inserting the notch filter into the forward path of the inner loop is the most appropriate way to suppress the natural vibration.

Author Contributions: Conceptualization, H.H.; Data curation, P.X.; Funding acquisition, K.L.; Investigation, H.H. and H.W.; Methodology, H.H.; Software, J.W.; Validation, H.W. and H.H.; Writing—original draft, H.H.; Writing—review and editing, H.W. and Y.Z. All authors have read and agreed to the published version of the manuscript.

Funding: Technology program of Shenzhen, China, under grants JCYJ20200109142205924 and 202001093000459.

Data Availability Statement: The data presented in this study are available upon request from the corresponding author. The data are not publicly available due to the privacy agreement among coauthors.

Conflicts of Interest: The authors declare no conflict of interest.

References

1. Komori, M.; Kato, H.; Asami, K.-I. Suspension-Type of Flywheel Energy Storage System Using High Tc Superconducting Magnetic Bearing (SMB). *Actuators* **2022**, *11*, 215. [[CrossRef](#)]
2. Hu, H.; Liu, K.; Wei, J.; Wang, H. Multirate model predictive current control of a permanent magnet synchronous machine for a flywheel energy storage system. *Energy Rep.* **2022**, *8*, 11579–11591. [[CrossRef](#)]
3. Shadnam ZARBIL, M.; Vahedi, A.; Azizi Moghaddam, H.; Khlyupin, P.A. Design and Sizing of Electric Bus Flash Charger Based on a Flywheel Energy Storage System: A Case Study. *Energies* **2022**, *15*, 8032. [[CrossRef](#)]
4. Farrokhzad Ershad, N.; Tafazzoli Mehrjardi, R.; Ehsani, M. High-Performance 4WD Electric Powertrain with Flywheel Kinetic Energy Recovery. *IEEE Trans. Power Electron.* **2021**, *36*, 772–784. [[CrossRef](#)]
5. Masouleh, M.I.; Limebeer, D.J.N. Fuel Minimization for a Vehicle Equipped With a Flywheel and Battery on a Three-Dimensional Track. *IEEE Trans. Intell. Veh.* **2017**, *2*, 161–174. [[CrossRef](#)]
6. Li, J.; Han, Y.; Li, S. Flywheel-Based Boom Energy Recovery System for Hydraulic Excavators with Load Sensing System. *Actuators* **2021**, *10*, 126. [[CrossRef](#)]
7. Hutchinson, A.; Gladwin, D.T. Optimisation of a wind power site through utilisation of flywheel energy storage technology. *Energy Rep.* **2020**, *6*, 259–265. [[CrossRef](#)]
8. Adhikari, S.; Karki, R.; Piya, P. Recovery Risk Mitigation of Wind Integrated Bulk Power System With Flywheel Energy Storage. *IEEE Trans. Power Syst.* **2019**, *34*, 3484–3493. [[CrossRef](#)]
9. Ghanaatian, M.; Lotfifard, S. Control of Flywheel Energy Storage Systems in the Presence of Uncertainties. *IEEE Trans. Sustain. Energy* **2019**, *10*, 36–45. [[CrossRef](#)]

10. Mukoyama, S.; Nakao, K.; Sakamoto, H.; Matsuoka, T.; Nagashima, K.; Ogata, M.; Yamashita, T.; Miyazaki, Y.; Miyazaki, K.; Maeda, T.; et al. Development of Superconducting Magnetic Bearing for 300 kW Flywheel Energy Storage System. *IEEE Trans. Appl. Supercond.* **2017**, *27*, 3600804. [[CrossRef](#)]
11. Werfel, F.N.; Floegel-Delor, U.; Riedel, T.; Rothfeld, R.; Wippich, D.; Goebel, B.; Reiner, G.; Wehlau, N. A Compact HTS 5 kWh/250 kW Flywheel Energy Storage System. *IEEE Trans. Appl. Supercond.* **2007**, *17*, 2138–2141. [[CrossRef](#)]
12. Gengji, W.; Ping, W. Rotor Loss Analysis of PMSM in Flywheel Energy Storage System as Uninterruptable Power Supply. *IEEE Trans. Appl. Supercond.* **2016**, *26*, 0609905. [[CrossRef](#)]
13. Nagorny, A.S.; Dravid, N.V.; Jansen, R.H.; Kenny, B.H. Design Aspects of a High Speed Permanent Magnet Synchronous Motor/Generator for Flywheel Applications. In Proceedings of the IEEE International Conference on Electric Machines & Drives, San Antonio, TX, USA, 15 May 2005.
14. Wang, P.; Gu, T.; Sun, B.; Liu, R.; Zhang, T.; Yang, J. Design and Performance Analysis of Super Highspeed Flywheel Rotor for Electric Vehicle. *World Electr. Veh. J.* **2022**, *13*, 147. [[CrossRef](#)]
15. Kale, V.; Secanell, M. A comparative study between optimal metal and composite rotors for flywheel energy storage systems. *Energy Rep.* **2018**, *4*, 576–585. [[CrossRef](#)]
16. Wang, H.; Wu, Z.; Liu, K.; Wei, J.; Hu, H. Modeling and Control Strategies of a Novel Axial Hybrid Magnetic Bearing for Flywheel Energy Storage System. *IEEE/ASME Trans. Mechatron.* **2022**, *27*, 3819–3829. [[CrossRef](#)]
17. Hu, H.; Liu, K.; Wang, H.; Wei, J. A Wide Bandwidth GaN Switching Power Amplifier of Active Magnetic Bearing for a Flywheel Energy Storage System. *IEEE Trans. Power Electron.* **2022**, *38*, 2589–2605. [[CrossRef](#)]
18. Wu, D.; Zhang, D.; Han, Q.; Wang, H. Study on nonlinear force transmissibility of flywheel rotor system considering periodic base motions. *J. Sound Vib.* **2022**, *529*, 116953. [[CrossRef](#)]
19. Herzog, R.; Buhler, P.; Gahler, C.; Larsonneur, R. Unbalance compensation using generalized notch filters in the multivariable feedback of magnetic bearings. *IEEE Trans. Control. Syst. Technol.* **1996**, *4*, 580–586. [[CrossRef](#)]
20. Zheng, S.; Han, B.; Feng, R.; Jiang, Y. Vibration Suppression Control for AMB-Supported Motor Driveline System Using Synchronous Rotating Frame Transformation. *IEEE Trans. Ind. Electron.* **2015**, *62*, 5700–5708. [[CrossRef](#)]
21. Cui, P.; Liu, Z.; Xu, H.; Zheng, S.; Han, B.; Zhang, D. Harmonic Vibration Force Suppression of Magnetically Suspended Rotor With Frequency-Domain Adaptive LMS. *IEEE Sens. J.* **2020**, *20*, 1166–1175. [[CrossRef](#)]
22. Li, J.; Liu, G.; Zheng, S.; Cui, P.; Chen, Q. Micro-Jitter Control of Magnetically Suspended Control Moment Gyro Using Adaptive LMS Algorithm. *IEEE/ASME Trans. Mechatron.* **2022**, *27*, 327–335. [[CrossRef](#)]
23. Chen, Q.; Liu, G.; Han, B. Unbalance vibration suppression for AMBs system using adaptive notch filter. *Mech. Syst. Signal Process.* **2017**, *93*, 136–150. [[CrossRef](#)]
24. Cui, P.; Li, S.; Wang, Q.; Gao, Q.; Cui, J.; Zhang, H. Harmonic Current Suppression of an AMB Rotor System at Variable Rotation Speed Based on Multiple Phase-Shift Notch Filters. *IEEE Trans. Ind. Electron.* **2016**, *63*, 6962–6969. [[CrossRef](#)]
25. He, J.; Deng, Z.; Peng, C.; Li, K. Reduction of the High-Speed Magnetically Suspended Centrifugal Compressor Harmonic Vibration Using Cascaded Phase-Shifted Notch Filters. *IEEE Sens. J.* **2021**, *21*, 1315–1323. [[CrossRef](#)]
26. Moir Tom, J. *Rudiments of Signal Processing and Systems*; Springer: Berlin/Heidelberg, Germany, 2022.

Disclaimer/Publisher’s Note: The statements, opinions and data contained in all publications are solely those of the individual author(s) and contributor(s) and not of MDPI and/or the editor(s). MDPI and/or the editor(s) disclaim responsibility for any injury to people or property resulting from any ideas, methods, instructions or products referred to in the content.